*Int. J. Heat Mass Transfer.* Vol. 30, No. 7, pp. 1331–1341, 1987
Printed in Great Britain

0017–9310/87 $3.00 + 0.00


# Onset of convection in a vertical slab of saturated porous media between two impermeable conducting blocks

M. WANG, D. R. KASSOY and P. D. WEIDMAN
Department of Mechanical Engineering, University of Colorado, Boulder, CO 80309, U.S.A.

(*Received* 8 *April* 1986 *and in final form* 10 *November* 1986)

**Abstract**—The onset of natural convection in a vertically oriented, finite thin slab of saturated porous material is considered. The slab is embedded between two impermeable conducting blocks of finite dimension. A vertical temperature difference is imposed between the upper and lower horizontal surfaces of the slab and blocks, and a linear temperature distribution is imposed on the outer vertical surfaces of the blocks. This configuration is used to model convection in a saturated, fractured rock zone like that associated with faulting. A linear stability analysis is developed for both convection in the slab and conduction in the block. The objective of the study is to obtain the critical Rayleigh number and mode of convection in the slab. When the block and the slab widths are both small compared to the other two dimensions one finds a large number of tall, narrow, three-dimensional cells. In contrast, a block of relatively large width promotes the formation of longer wavelength, weakly three-dimensional cells in the slab at a much lower Rayleigh number. The difference is related to the character of the temperature distribution in the solid block.

## 1. INTRODUCTION

THE SUBJECT of buoyancy induced convection in saturated porous media has been widely studied in the last three decades, motivated by engineering technology and geophysical problems as well as basic scientific interest. Early attempts emphasize convection processes in infinite and confined porous material between horizontal surfaces with an imposed temperature difference (e.g. refs. [1, 2]). The sidewalls are assumed to be insulated. Except for vertical columnar geometries, the critical Rayleigh number for onset of convection in such systems is usually $R_c = 4\pi^2$ or in the vicinity of that value.

In many practical situations, horizontal heat exchange through vertical confining boundaries may be as important as the heat transfered vertically through the porous media. Then the traditional insulated boundary condition is inappropriate. This fact has inspired several investigators to develop an understanding of the effects of sidewall heat transfer on the character of convection in porous media, and to determine the conditions necessary for the onset of convection and the mode configurations. A few examples of these analyses are given by Lowell and Shyu [3], Murphy [4], Kassoy and Cotte [5] and Weidman and Kassoy [6]. In the most recent studies [5, 6], the onset of natural convection in a vertically oriented, thin, finite slab of saturated porous media is considered. Heat flow is allowed through the broad vertical sidewalls but not through the narrow endwalls. A linear stability analysis is carried out and results are obtained from an asymptotic evaluation of the exact stability criteria in the limit of small gap width $\varepsilon \to 0$, where $\varepsilon$ is the ratio of the narrow horizontal dimension of the slab to its height. The analysis shows that when the appropriately defined Biot number is $O(1)$, including the case $B \to \infty$, the critical Rayleigh number $R_c = O(\varepsilon^{-2})$. The convection mode consists of tightly-packed three-dimensional cells with a wave number $\alpha_c = O(\varepsilon^{-1/2})$. Only when the Biot number is sufficiently small, $O(\varepsilon^2)$, are the classical results for adiabatic sidewalls, $R_c = 4\pi^2$, $\alpha_c = \pi$, approached. One distinct advantage of the analyses in refs. [5, 6] is that, unlike earlier efforts, the mathematical formulation as well as the solutions are based on a fully three-dimensional model, in which an eigenfunction describes the temperature variation in the cross-slab direction. Such a treatment ensures a degree of resolution not possible with Murphy's two-dimensional analysis [4]. The results in refs. [5, 6] agree with Murphy's qualitatively in the sense that both show the strong stabilizing effect of sidewall heat transfer.

In the work by Weidman and Kassoy [6], one should notice that the thermal conditions on the sidewalls are controlled by a single parameter, the Biot number, which arises from a boundary condition relating the temperature to the temperature gradient on the slab wall. In this sense the thermal response of the material external to the slab is ignored. In reality, the porous slab is usually found embedded in a larger environment with a characteristic heat transfer that produces a strong feedback on the convection in the slab. One such example is a fault zone of fractured rock embedded in impermeable material which is presumed to extend far away in the horizontal direction. The purpose of this study is to describe the thermal interactions between the environment and the porous slab and their influence on criticality behavior. We consider a slab embedded between two impermeable

## NOMENCLATURE

| | |
|---|---|
| $c$ | specific heat of fluid |
| $D$ | block width |
| $\bar{D}$ | scaled block width, $D/\varepsilon$ |
| $f(\bar{y}, \alpha, \hat{R}, \varepsilon)$ | cross-slab eigenfunction |
| $f_b(y)$ | cross-block function |
| $g$ | gravitational acceleration |
| $H_1$ | slab length |
| $H_2$ | slab width |
| $H_{1tr}$ | transitional slab length |
| $k$ | permeability of the porous medium |
| $K$ | ratio of block to liquid saturated porous matrix thermal conductivities, $\lambda_b'/\lambda_m'$ |
| $l$ | horizontal wavelength, $2\pi/\alpha$ |
| $L$ | slab height |
| $p$ | fluid pressure |
| $P$ | characteristic pressure defined by equation (4h) |
| $R$ | Rayleigh number defined in equation (4f) |
| $\bar{R}$ | scaled Rayleigh number, $\varepsilon^2 R$ |
| $\hat{R}$ | scaled Rayleigh number, $\varepsilon R$ |
| $T$ | temperature |
| $T_0$ | temperature at the upper surface |
| $T_1$ | temperature at the lower surface |
| $u$ | fluid velocity in the $x$-direction |
| $U$ | characteristic velocity defined by equation (4g) |
| $v$ | fluid velocity in the $y$-direction |
| $w$ | fluid velocity in the $z$-direction |
| $(x, y)$ | horizontal coordinates |
| $\bar{y}$ | scaled horizontal coordinate, $y/\varepsilon$ |
| $Y_P$ | penetration depth of temperature disturbance in the block |
| $z$ | vertical coordinate. |

Greek symbols

| | |
|---|---|
| $\alpha$ | horizontal wave number |
| $\bar{\alpha}$ | scaled horizontal wave number, $\varepsilon^{1/2}\alpha$ |
| $\beta$ | volume expansion coefficient of the fluid |
| $\varepsilon$ | dimensionless slab width, $H_2'/L'$ |
| $\theta$ | disturbance temperature |
| $\lambda$ | thermal conductivity |
| $\Lambda$ | quantity defined by equation (A3) |
| $\nu$ | kinematic viscosity of the fluid |
| $\rho_0$ | density of the fluid evaluated at the upper surface temperature $T_0'$ |
| $\tau$ | overheat ratio, $(T_1'-T_0')/T_0'$. |

Subscripts

| | |
|---|---|
| b | conducting block |
| c | critical value |
| m | fluid-saturated porous matrix |
| $(x, y, z)$ | $(x, y, z)$-derivative. |

Superscripts

| | |
|---|---|
| $(\ )'$ | dimensional quantity |
| * | terms in the $R_c$ expansions after expanding the wave number. |

conducting blocks. It will be shown that the critical Rayleigh number and the modal configuration of convection differ fundamentally from those found in previous studies [5, 6] where direct thermal interaction with the environment is not admitted.

## 2. PROBLEM FORMULATION AND SOLUTION

We consider the onset of buoyancy induced convection in a slab embedded between two impermeable conducting blocks as shown in Fig. 1. The dimensions of the slab are specified by height $L'$, length $H_1'$, and width $H_2'$. Two adjacent blocks with the same lengths and heights as the slab extend a distance $D'$ horizontally away from opposite sides of the slab. The upper and lower surfaces of this sandwiched system are maintained at temperatures $T_0'$ and $T_1'$, respectively, such that $\Delta T' = T_1' - T_0' > 0$. The front and rear surfaces including the two endwalls of the slab, on the other hand, are assumed to be insulated. It is also assumed that the temperature increases linearly with depth at the far side of each block (cf. Fig. 1), namely

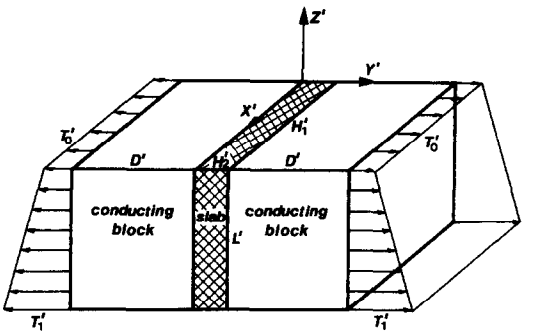


FIG. 1. Geometry and coordinates for the embedded vertical slab of saturated porous media.

$T' = T_0' - \Delta T' z'/L'$. In addition, the six walls of the slab are impermeable.

### 2.1. *Linear stability analysis for the slab*

The non-dimensional equations for conservation of mass, momentum and energy in the porous slab are given by [5]

$$u_x + v_y + w_z = 0 \tag{1}$$

$$u = -p_x, \quad v = -p_y, \quad w = -p_z + \frac{T-1}{\tau} \tag{2a–c}$$

$$R[uT_x + vT_y + wT_z] = T_{xx} + T_{yy} + T_{zz}. \tag{3}$$

The dimensionless variables are defined by

$$(x, y, z) = \frac{(x', y', z')}{L'}, \quad (u, v, w) = \frac{(u', v', w')}{U'} \tag{4a, b}$$

$$T = \frac{T'}{T'_0}, \quad p = \frac{p' + \rho'_0 g' z'}{P'} \tag{4c, d}$$

$$\tau = \frac{T'_1 - T'_0}{T'_0}, \quad R = \frac{\rho'_0 g' \beta' \Delta T' k' c' L'}{\lambda'_m \nu'} \tag{4e, f}$$

where $c'$ is the specific heat of the fluid, $\lambda'_m$ the thermal conductivity of the fluid-saturated porous matrix, $\rho'_0$ the fluid density evaluated at temperature $T'_0$, and $g'$ represents the gravitational acceleration. The characteristic velocity and pressure for this system are

$$U' = k' g' \beta' \Delta T' / \nu' \quad \text{and} \quad P' = \rho'_0 g' \beta' L' \Delta T' \tag{4g, h}$$

respectively. In the derivation of equations (1)–(3), a Boussincsq fluid of constant kinematic viscosity $\nu'$, volume expansion coefficient $\beta'$ and specific heat $c'$ is assumed. The thermal conductivity $\lambda'_m$ and the permeability $k'$ are also assumed constant.

The boundary conditions for the geometry sketched in Fig. 1 are

$$z = 0 \qquad w = 0, \quad T = 1 \tag{5a}$$

$$z = -1 \qquad w = 0, \quad T = 1 + \tau \tag{5b}$$

$$x = 0, H_1 \quad u = 0, \quad T_x = 0 \tag{5c}$$

$$y = 0, H_2 \quad v = 0, \quad T = T_b, \quad T_y = K T_{by} \tag{5d}$$

where $(H_1, H_2) = (H'_1, H'_2)/L'$ are the two horizontal aspect ratios describing the porous slab geometry. The ratio of block to saturated porous matrix thermal conductivities is $K = \lambda'_b/\lambda'_m = O(1)$. The latter is assumed to be a material property of the system. Subscript b has been introduced and will be used throughout the subsequent analysis to denote properties associated with the conducting block. Thermal boundary condition (5d) assumes the continuity of temperature and heat flux at the slab–block interfaces.

First we develop a linear stability analysis for equations (1)–(3), subject to boundary conditions (5a)–(5d). Coupling between the slab and block temperatures, represented by thermal conditions (5d), will be included later in conjunction with the describing system for conducting blocks. Following the procedures developed in refs. [5, 6], the temperature disturbance $\theta$ is defined by

$$T = 1 - \tau z + \tau\theta. \tag{6}$$

Since the problem is to be solved explicitly for a thin slab in the limit $H_2 \to 0$, we define $H_2 \equiv \varepsilon$. The magnitude of the global minimum Rayleigh number, for the configuration and boundary conditions employed, is found to be $R = O(\varepsilon^{-1})$, a value intermediate between that for the insulated case, $R = O(1)$ [1], and that for the perfectly conducting sidewall, $R = O(\varepsilon^{-2})$ [5]. Scaled values

$$\bar{y} = y/\varepsilon, \quad \hat{R} = \varepsilon R \tag{7}$$

can be used to construct the exact temperature disturbance equation and boundary conditions from equations (1)–(3) and (5)

$$\varepsilon^4(\theta_{xxxx} + \theta_{zzzz} + 2\theta_{xxzz}) + \varepsilon^3 \hat{R}\theta_{xx} + \varepsilon^2(2\theta_{xx\bar{y}\bar{y}} + 2\theta_{zz\bar{y}\bar{y}}) + \varepsilon\hat{R}\theta_{\bar{y}\bar{y}} + \theta_{\bar{y}\bar{y}\bar{y}\bar{y}} = 0 \tag{8a}$$

$$z = 0, -1 \qquad \theta = \theta_{zz} = 0 \tag{8b}$$

$$x = 0, H_1 \qquad \theta_x = \theta_{xxx} = 0 \tag{8c}$$

$$\bar{y} = 0, 1 \quad \varepsilon^2(\theta_{xx\bar{y}} + \theta_{zz\bar{y}}) + \varepsilon\hat{R}\theta_{\bar{y}} + \theta_{\bar{y}\bar{y}\bar{y}} = 0. \tag{8d}$$

A separable solution containing the most unstable modes can be written as

$$\theta(x, \bar{y}, z) = \sin \pi z \cos \alpha x \, f(\bar{y}; \alpha, \hat{R}, \varepsilon). \tag{9}$$

The ordinary differential equation for the cross-slab eigenfunction and the boundary conditions corresponding to (8d) are given by

$$f^{(4)}(\bar{y}) + [\varepsilon\hat{R} - 2\varepsilon^2(\pi^2 + \alpha^2)]f''(\bar{y}) + [\varepsilon^4(\pi^2 + \alpha^2)^2 - \varepsilon^3\alpha^2\hat{R}]f(\bar{y}) = 0 \tag{10a}$$

$$\bar{y} = 0, 1 \quad f'''(\bar{y}) + [\varepsilon\hat{R} - \varepsilon^2(\pi^2 + \alpha^2)]f'(\bar{y}) = 0. \tag{10b}$$

The wave number $\alpha$, determined by putting equation (9) into (8c), takes the form

$$\alpha = \frac{m\pi}{H_1} \quad m = 0, 1, 2, \ldots \tag{11}$$

The two remaining boundary conditions necessary for solution of equation (10a) are found from thermal continuity conditions (5d). Therefore, it is necessary at this point to consider the heat conduction processes in the block. A linear stability analysis is to be carried out for the block lying to the left of the slab (cf. Fig. 1), with the objective of finding the appropriate left surface boundary condition for $f(\bar{y})$. The boundary condition on the opposite side can be obtained by symmetry arguments.

### 2.2. *Linear stability analysis for the block*

The dimensionless heat conduction equation and boundary conditions for the block may be written as

$$T_{bxx} + T_{byy} + T_{bzz} = 0 \tag{12a}$$

$$x = 0, H_1 \quad T_{bx} = 0 \tag{12b}$$

$$z = 0 \qquad T_b = 1 \tag{12c}$$

$$z = -1 \qquad T_b = 1 + \tau \tag{12d}$$

$$y = -D \qquad T_b = 1 - \tau z \tag{12e}$$

$$y = 0 \qquad T_b = T, \quad T_{by} = (1/K)T_y \tag{12f}$$

where $D = D'/L'$ is the dimensionless block width.

The conditions at $y = 0$ are taken from (5d). The describing system for the disturbance temperature $\theta_b$ in the block is

$$\theta_{bxx} + \theta_{byy} + \theta_{bzz} = 0 \quad (13a)$$

$$x = 0, H_1 \quad \theta_{bx} = 0 \quad (13b)$$

$$z = 0, -1 \quad \theta_b = 0 \quad (13c)$$

$$y = -D \quad \theta_b = 0 \quad (13d)$$

$$y = 0 \quad \theta_b = \theta \quad (13e)$$

$$y = 0 \quad \theta_{by} = (1/\varepsilon K)\theta_{\bar{y}} \quad (13f)$$

where $\theta_b$ is defined by

$$T_b = 1 - \tau z + \tau\theta_b. \quad (14)$$

The small aspect ratio $\varepsilon$ appearing in equation (13f) is due to the different $y$-scalings used in the block and in the slab. Again, a separated solution

$$\theta_b = \sin \pi z \cos \alpha x \, f_b(y) \quad (15)$$

is used to find the cross-block function $f_b(y)$ equation and boundary conditions

$$f_b''(y) - (\pi^2 + \alpha^2) f_b(y) = 0 \quad (16a)$$

$$f_b(0) = f(0) \quad (16b)$$

$$f_b(-D) = 0. \quad (16c)$$

The exact solution is found to be

$$f_b(y) = \frac{f(0)}{\sinh [D(\pi^2+\alpha^2)^{1/2}]} \times \sinh [(y+D)(\pi^2+\alpha^2)^{1/2}] \quad (17)$$

and

$$f_{by}(0) = f(0)(\pi^2+\alpha^2)^{1/2} \coth [D(\pi^2+\alpha^2)^{1/2}]. \quad (18)$$

It follows from equations (9), (13f), (15) and (18) that

$$f_{\bar{y}}(0) = \varepsilon K(\pi^2+\alpha^2)^{1/2} \coth [D(\pi^2+\alpha^2)^{1/2}] f(0). \quad (19)$$

An application of the same analytical procedure to the block lying to the right of the slab gives the anti-symmetrical boundary condition

$$f_{\bar{y}}(1) = -\varepsilon K(\pi^2+\alpha^2)^{1/2} \coth [D(\pi^2+\alpha^2)^{1/2}] f(1). \quad (20)$$

Equations (19) and (20) depend only on $f(\bar{y})$ and provide the remaining boundary conditions necessary to close the problem represented by equations (10).

### 2.3. *The general solution*

Equations (10), (19) and (20) form a complete system describing the cross-slab eigenfunction. They are summarized here to facilitate the subsequent analysis

$$f^{(4)}(\bar{y}) + [\varepsilon\hat{R} - 2\varepsilon^2(\pi^2+\alpha^2)] f''(\bar{y}) + [\varepsilon^4(\pi^2+\alpha^2)^2 - \varepsilon^3\alpha^2\hat{R}] f(\bar{y}) = 0 \quad (21a)$$

$$f'(0) - \varepsilon K(\pi^2+\alpha^2)^{1/2} \coth [D(\pi^2+\alpha^2)^{1/2}] f(0) = 0 \quad (21b)$$

$$f'''(0) + [\varepsilon\hat{R} - \varepsilon^2(\pi^2+\alpha^2)] f'(0) = 0 \quad (21c)$$

$$f'(1) + \varepsilon K(\pi^2+\alpha^2)^{1/2} \coth [D(\pi^2+\alpha^2)^{1/2}] f(1) = 0 \quad (21d)$$

$$f'''(1) + [\varepsilon\hat{R} - \varepsilon^2(\pi^2+\alpha^2)] f'(1) = 0. \quad (21e)$$

Boundary conditions (21b) and (21d) specify heat exchange through the sidewalls of the slab. Note that the heat transfer rate is a function of several parameters; thermal conductivity ratio, slab width, and more importantly, the wave number, in contrast to the case studied by Weidman and Kassoy [6], where the wave number is absent in the heat transfer boundary conditions. The strong wave number dependence of the boundary heat flux forms a unique feature of the current problem. It arises from the $x$-direction heat conduction in the block which has not been considered in earlier studies. The cellular convection mode in the slab affects the heat conduction character in the neighboring solid block, which in turn strongly influences heat transfer between the two environments.

The exact solution to equations (21) can be written in the form (cf. Kassoy and Cotte [5])

$$f(\bar{y}) = \sin \lambda\bar{y} + E \cos \lambda\bar{y} + F \sinh \gamma\bar{y} + G \cosh \gamma\bar{y} \quad (22)$$

where

$$\lambda = \left\{ \frac{\varepsilon\hat{R}}{2} \left[ 1 + \left( 1 - \frac{4\pi^2\varepsilon}{\hat{R}} \right)^{1/2} \right] - \varepsilon^2(\pi^2+\alpha^2) \right\}^{1/2} \quad (23)$$

$$\gamma = \left\{ -\frac{\varepsilon\hat{R}}{2} \left[ 1 - \left( 1 - \frac{4\pi^2\varepsilon}{\hat{R}} \right)^{1/2} \right] + \varepsilon^2(\pi^2+\alpha^2) \right\}^{1/2}. \quad (24)$$

In order to satisfy boundary conditions (21b)–(21e)

$$E = \frac{D_1B_2 - D_2B_1}{A_1B_2 - A_2B_1}, \quad F = \frac{\lambda(\lambda^2 - S)}{\gamma(\gamma^2 + S)}$$

$$G = \frac{A_1D_2 - A_2D_1}{A_1B_2 - A_2B_1} \quad (25a\text{–}c)$$

$$[D_1(B_2 - A_2) + D_2(A_1 - B_1)]C(\gamma^2 + S) = (A_1B_2 - A_2B_1)\lambda(\lambda^2 + \gamma^2) \quad (26)$$

$$A_1 = \lambda(\lambda^2 - S) \sin \lambda, \quad A_2 = -\lambda \sin \lambda + C \cos \lambda \quad (27a,b)$$

$$B_1 = \gamma(\gamma^2 + S) \sinh \gamma, \quad B_2 = \gamma \sinh \gamma + C \cosh \gamma \quad (28a,b)$$

$$D_1 = \lambda(\lambda^2 - S)(\cos \lambda - \cosh \gamma) \quad (29a)$$

$$D_2 = -C \sin \lambda - \lambda \cos \lambda - (C \sinh \gamma + \gamma \cosh \gamma)F \quad (29b)$$

$$C = \varepsilon K(\pi^2+\alpha^2)^{1/2} \coth [D(\pi^2+\alpha^2)^{1/2}] \quad (30)$$

$$S = \varepsilon\hat{R} - \varepsilon^2(\pi^2+\alpha^2). \quad (31)$$

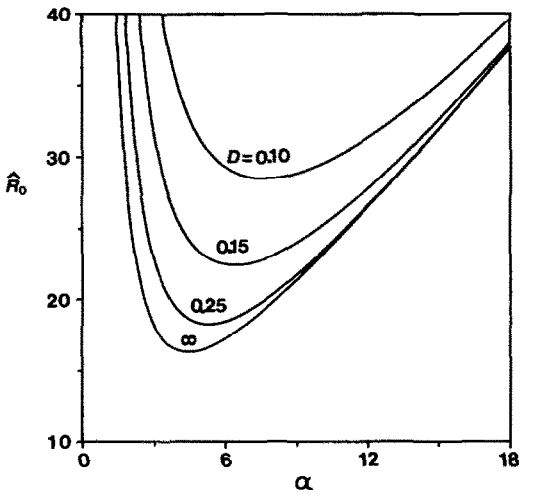


FIG. 2(a). The variation of the lowest order Rayleigh number approximation $\hat{R}_0$ with the wave number $\alpha$ for several block widths $D$. The conductivity ratio is $K = 1$.

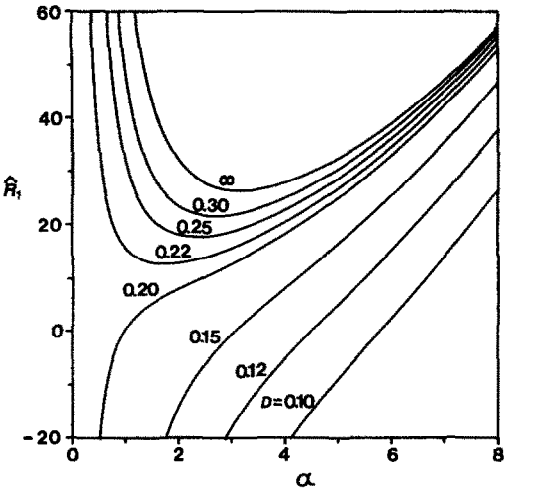


FIG. 2(b). The variation of the first-order Rayleigh number approximation $\hat{R}_1$ with the wave number $\alpha$ for several block widths $D$. The conductivity ratio is $K = 1$.

Equation (26) is the exact eigenvalue equation for the Rayleigh number in terms of the parameters defined above. Since our main concern is the stability criterion for the onset of convection in the slab, equation (26) is to be evaluated by a regular perturbation procedure in the thin slab limit $\varepsilon \to 0$.

2.4. *Asymptotic analysis*

When $K = O(1)$ and $D = O(1)$, a distinguished limit can be found for $\alpha = O(1)$ and $\hat{R} = O(1)$. If the scaled Rayleigh number is written as

$$\hat{R} = \hat{R}_0 + \varepsilon \hat{R}_1 + O(\varepsilon^2) \tag{32}$$

then a systematic expansion of equation (26) leads to an ordered set of equations in powers of $\varepsilon$. Solutions of the first two may be written in the form

$$\hat{R}_0 = \frac{2K(\pi^2+\alpha^2)^{3/2} \coth [D(\pi^2+\alpha^2)^{1/2}]}{\alpha^2} \tag{33}$$

$$\hat{R}_1 = \frac{3-K^2 \coth^2 [D(\pi^2+\alpha^2)]}{3} \frac{(\pi^2+\alpha^2)^2}{\alpha^2} \tag{34}$$

and are plotted in Figs. 2(a) and (b) for the special case of $K = 1$ and a set of selected values of $D$. The basic approximation $\hat{R}_0$ increases as the block width decreases as a result of increased heat exchange between the block and slab. This lowest order stabilization effect is reduced slightly by the $\varepsilon \hat{R}_1$ term which, for a given $\varepsilon$-value, decreases as $D$ is reduced. One should also note that the basic Rayleigh number approximation increases linearly with $K$. Here again increased stabilization follows from enhancement of heat exchange between the slab and the environment. In contrast, there is a much weaker destabilizing influence from $\varepsilon \hat{R}_1$ as $K$ is increased. Given a specific value of $\varepsilon$, one can form neutral stability curves of second-order accuracy by a combination of results in equations (32)–(34).

An inspection of the above results indicates that expansion (32) is uniformly valid in the range $O(\varepsilon) < D < \infty$. When $D = O(\varepsilon)$, however, the magnitude of the second term in expansion (32) becomes comparable with that of the first, and the limit-process expansion fails to be valid.

The critical values of $\hat{R}$ and $\alpha$ are determined by using the condition $d\hat{R}/d\alpha = 0$. The expanded critical wave number

$$\alpha_c = \alpha_{0c} + \varepsilon \alpha_{1c} + O(\varepsilon^2) \tag{35}$$

is used in the derivative condition together with expansion (32). We find

$$\hat{R}_c = \hat{R}^*_{0c}(\alpha_{0c}) + \varepsilon \hat{R}^*_{1c}(\alpha_{0c}, \alpha_{1c}) + O(\varepsilon^2) \tag{36}$$

where the asterisk denotes terms after expanding the wave number. An implicit relation is found for $\alpha_{0c}$

$$\alpha_{0c}^2 \left\{ 1 - \frac{2D(\pi^2+\alpha_{0c}^2)^{1/2}}{\sinh [2D(\pi^2+\alpha_{0c}^2)^{1/2}]} \right\} = 2\pi^2 \tag{37}$$

and $\hat{R}^*_{0c}$ follows from equation (33)

$$\hat{R}^*_{0c} = \frac{2K(\pi^2+\alpha_{0c}^2)^{3/2} \coth [D(\pi^2+\alpha_{0c}^2)^{1/2}]}{\alpha_{0c}^2}. \tag{38}$$

Expressions for first-order terms $\alpha_{1c}$ and $\hat{R}^*_{1c}$ are rather lengthy and are listed in the Appendix for the interested reader's reference. Values of $\alpha_{0c}$, $\alpha_{1c}$, $\hat{R}^*_{0c}$ and $\hat{R}^*_{1c}$ have been found numerically for different values of $D$ in the special case when $K = 1$. They are plotted in Figs. 3(a) and (b). Some typical values are listed in Table 1 so that quantitative critical results for instability can be obtained. It is observed that the influence of block width $D$ on these critical values is confined to a narrow region near zero block thickness. As soon as $D$ reaches approximately 0.5, these values do not differ appreciably from those corresponding to the asymptotic limit $D \to \infty$.

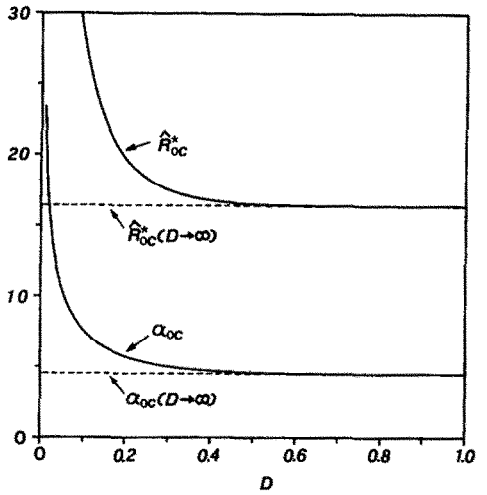


FIG. 3(a). The variations of the lowest order critical values of $\hat{R}^*_{0c}$ and $\alpha_{0c}$ with the block width $D$. The asymptotes for $D \to \infty$ are represented by dashed lines. The conductivity ratio is $K = 1$.

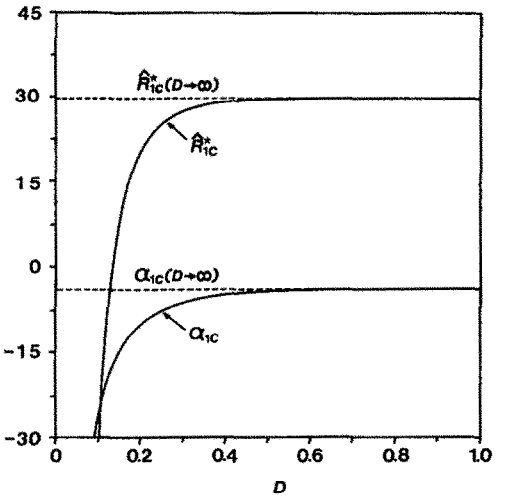


FIG. 3(b). The variations of the first-order critical values of $\hat{R}^*_{1c}$ and $\alpha_{1c}$ with the block width $D$. The asymptotes for $D \to \infty$ are represented by dashed lines. The conductivity ratio is $K = 1$.

Table 1. Critical values ($K = 1$)

| $D$ | $\alpha_{0c}$ | $\hat{R}^*_{0c}$ | $\alpha_{1c}$ | $\hat{R}^*_{1c}$ |
|---|---|---|---|---|
| 0.02 | 16.56 | 107.49 | −279.84 | −2256.29 |
| 0.04 | 11.77 | 57.73 | −100.66 | −492.81 |
| 0.06 | 9.67 | 41.31 | −55.72 | −182.54 |
| 0.08 | 8.43 | 33.23 | −36.80 | −79.34 |
| 0.10 | 7.61 | 28.47 | −26.77 | −33.97 |
| 0.14 | 6.56 | 23.25 | −16.73 | 2.76 |
| 0.20 | 5.68 | 19.68 | −10.38 | 19.89 |
| 0.30 | 4.99 | 17.45 | −6.41 | 27.13 |
| 0.50 | 4.54 | 16.46 | −4.38 | 29.37 |
| 1.00 | 4.44 | 16.32 | −4.03 | 29.61 |
| ∞ | 4.44 | 16.32 | −4.03 | 29.61 |

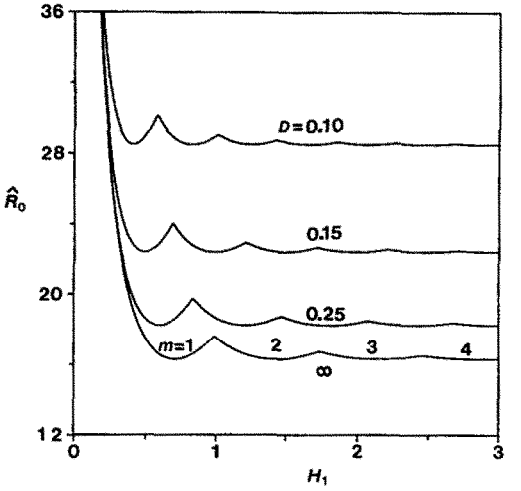


FIG. 4. The variation of $\hat{R}_0$ with $H_1$ for several values of $D$ when $K = 1$. The preferred mode numbers $m$ are indicated.

Onset of motion in the slab will occur at the critical conditions computed above as long as the wave fitting condition (11) is met. In general, however, for a given slab aspect ratio $H_1$, since only an integer number of modes are allowed, motion will occur according to the neutral stability criteria in equations (32)–(34). When the value of $H_1$ is changed continuously, new modes appear or existing modes vanish to fit the system with the lowest Rayleigh number. The transition from $m$ to $m+1$ modes occurs when $\hat{R}(\alpha_m) = \hat{R}(\alpha_{m+1})$.

To a first approximation, it follows from equations (33) and (11) that

$$\frac{(\pi^2+\alpha_m^2)^{3/2}\coth\left[D(\pi^2+\alpha_m^2)^{1/2}\right]}{\alpha_m^2} = \frac{(\pi^2+\alpha_{m+1}^2)^{3/2}\coth\left[D(\pi^2+\alpha_{m+1}^2)^{1/2}\right]}{\alpha_{m+1}^2} \tag{39}$$

and

$$[H_{1tr}^2+m^2]^{3/2}(m+1)^2\tanh\left\{\pi D\left[1+\frac{(m+1)^2}{H_{1tr}^2}\right]^{1/2}\right\} = [H_{1tr}^2+(m+1)^2]^{3/2}m^2\tanh\left\{\pi D\left[1+\frac{m^2}{H_{1tr}^2}\right]^{1/2}\right\} \tag{40}$$

where $H_{1tr}$ denotes the slab aspect ratio at which mode transition occurs.

In Fig. 4, the neutral stability curves and the transition aspect ratio are given for selected values of $D$. For a specified slab geometry, decreasing the block width tends to increase the modal wave number $\alpha$; that is, the convection pattern is composed of a greater number of necessarily thinner cells.

### 2.5. *The special case of large D: application to geothermal systems*

The foregoing analysis can be greatly simplified if we consider the case where the block width is comparable to or larger than its depth because

$\coth[D(\pi^2+\alpha^2)^{1/2}] = 1$ as $D \to \infty$. In fact, when $D = 0.5$ and $\alpha_c \simeq 4.44$ as calculated above, then $\coth[D(\pi^2+\alpha^2)^{1/2}] \simeq 1.01$. This result shows that when $D$ is sufficiently large, there is practically no distinction between finite block width and infinite block width as far as the stability properties within the thin slab are concerned. When $\coth[D(\pi^2+\alpha^2)^{1/2}]$ is replaced by 1 in equations (21b) and (21d), the system for the slab eigenfunction becomes independent of $D$. In this case, the desired critical stability results for the onset of convection in the porous slab can be found analytically as explicit functions of system parameters. These limiting results are given below.

(a) Neutral stability curve:

$$\hat{R} = \frac{2K(\pi^2+\alpha^2)^{3/2}}{\alpha^2} + \frac{3-K^2}{3}\frac{(\pi^2+\alpha^2)^2}{\alpha^2}\varepsilon + O(\varepsilon^2). \tag{41}$$

(b) Critical Rayleigh number:

$$\hat{R}_c = \hat{R}^*_{0c} + \hat{R}^*_{1c}\varepsilon + O(\varepsilon^2) = 3\sqrt{3\pi K} + \frac{3\pi^2(3-K^2)}{2}\varepsilon + O(\varepsilon^2). \tag{42}$$

(c) Critical wave number:

$$\alpha_c = \alpha_{0c} + \alpha_{1c}\varepsilon + O(\varepsilon^2) = \sqrt{2\pi} + \frac{(K^2-3)\pi^2}{2\sqrt{6K}}\varepsilon + O(\varepsilon^2). \tag{43}$$

(d) Transitional slab aspect ratio:

$$H_{1tr} = \left[\frac{(m+1)^2 m^{4/3} - m^2(m+1)^{4/3}}{(m+1)^{4/3} - m^{4/3}}\right]^{1/2}. \tag{44}$$

For comparison, these $D \to \infty$ results have been plotted in Figs. 2–4 for $K = 1$ together with results obtained for various finite values of $D$. It is seen clearly from Figs. 3(a) and (b) that departures in critical values from the infinite block width case become insignificant when $D > 0.5$.

An important application of this study is to the heat and mass transport in geothermal systems where vertical faults of permeable material are known to be present [8]. The establishment of convection in these faults can increase the local heat transport by orders of magnitude, in comparison to pure conduction [7]. Hence the conditions for the occurrence of convection are of considerable interest. Our mathematical model is expected to provide a good prediction for those criticality results because it relies on fewer approximations than used in earlier studies. Most importantly, we have developed a three-dimensional model of convection and accounted for the effect of rock heat conduction induced by thermal disturbances in the water-saturated material. In geothermal systems associated with fault zones the assumption of large width to height ratio is valid, and equations (42) and (43) should provide a realistic estimation of critical values.

A sample calculation is carried out for a narrow fault zone embedded between rock masses of much larger lateral extent. Both sandstone and limestone, with markedly different thermal conductivities, are considered. As a rough estimate, the same matrix thermal conductivity is used in both cases; $\lambda_m = 1.2\,\mathrm{W\,m^{-1}\,^\circ C^{-1}}$ [8]. The critical Rayleigh number $R_c$ and critical non-dimensional wavelength defined by $l_c = 2\pi/\alpha_c$ can be computed. Table 2 lists values for several dimensionless fault widths. The stabilizing effect of increasing thermal conductivity ratio $K$ or decreasing dimensionless fault width $\varepsilon$, both implying increasing heat exchange per unit mass of fluid with the surrounding rock, should be observed. Finally, one may note that $R_c$ always exceeds the minimum classical value $4\pi^2$ which is found only when there is no heat transfer to the bounding solid rock.

## 3. DISCUSSION

The preceding asymptotic calculations show that when the conductivity ratio $K = O(1)$, then the Rayleigh number $R = O(\varepsilon^{-1})$ for onset of motion in the physical system described in Fig. 1. This result, when compared to that for the fully insulated case where $R = O(1)$ (e.g. see Zebib and Kassoy [2]), demonstrates that sidewall heat transfer is a stabilizing influence. The stabilizing effect for the embedded slab is much weaker than that found when a heat transfer condition is applied directly to the sidewall. For the latter case [5], the onset Rayleigh number $R = O(\varepsilon^{-2})$.

The convection mode, on the other hand, does not exhibit a horizontal wave number intermediate between those found in refs. [2, 5]. Rather one finds $O(1)$ wave number cells similar to those in the fully-insulated case. This surprising result can be attributed to the diffusion of heat in the solid block along the plane of the interface between the block and the slab which tends to smooth out thermal gradients associated with large wave number patterns. In other words, a narrow cell with relatively large horizontal temperature gradients along the slab, is not compatible with the conduction process in the block when $D = O(1)$. In contrast, when $D = O(\varepsilon)$, so that the thermal boundary condition is applied close to the interface, as will be shown, the convection mode consists of narrow, three-dimensional cells.

In order to obtain a thorough understanding of the predicted $O(1)$ wave number convection cell we examine in detail its structural properties in the cross-slab direction. The eigenfunction, obtained directly from equations (21), has the form

$$f(\bar{y}) = 1 + \{K(\pi^2+\alpha^2)^{1/2}\coth[D(\pi^2+\alpha^2)^{1/2}]\}\bar{y}(1-\bar{y})\varepsilon + O(\varepsilon^2). \tag{45a}$$

Equation (45a) can be evaluated at the critical values,

Table 2. Critical values for onset of convection in faults

| Environmental material | Thermal conductivity $\lambda$ (W m$^{-1}$ °C$^{-1}$) (adapted from ref. [9]) | (Fault width)/(Height) $\varepsilon$ | Critical Rayleigh number $R_c$ | Critical wavelength $l_c$ |
|---|---|---|---|---|
| Sandstone | $\lambda_b = 1.8$ ($K = 1.5$) | 0.1 | $2.6 \times 10^2$ | 1.45 |
| | | 0.01 | $2.5 \times 10^3$ | 1.42 |
| | | 0.001 | $2.4 \times 10^4$ | 1.41 |
| Limestone | $\lambda_b = 1.2$ ($K = 1.0$) | 0.1 | $1.9 \times 10^2$ | 1.55 |
| | | 0.01 | $1.7 \times 10^3$ | 1.43 |

equations (37) and (38), to find the critical eigenfunction

$$f_c(\bar{y}) = 1 + \frac{\alpha_{0c}^2 \hat{R}_{0c}^*}{2(\pi^2 + \alpha_{0c}^2)} \bar{y}(1-\bar{y})\varepsilon + O(\varepsilon^2). \quad (45b)$$

For the case of large block width $D$, one finds from equations (42) and (43)

$$f_c(\bar{y}) = 1 + \sqrt{3}\pi K \bar{y}(1-\bar{y})\varepsilon + O(\varepsilon^2). \quad (45c)$$

The critical eigenfunction exhibits a variation with $\bar{y}$ in the $O(\varepsilon)$ term. Small as it is in the absolute sense, the variation is of the magnitude of the slab width. This implies that temperature changes per unit distance in a convection cell are of the same order of magnitude in all three directions. Clearly, it is inappropriate to characterize these unstable modes as two-dimensional rolls, as in the case of insulated sidewalls. Rather we choose to call them tall, large, weakly three-dimensional convection cells.

Also of interest is the cross-block function $f_b(y)$, since it reveals the nature of the temperature field in the blocks. In the block lying to the left of the slab, this function is given by equations (17) and (45)

$$f_b(y) = \frac{\sinh[(y+D)(\pi^2+\alpha^2)^{1/2}]}{\sinh[D(\pi^2+\alpha^2)^{1/2}]} \quad (46a)$$

with

$$f_b(y) \to \exp[y(\pi^2+\alpha^2)^{1/2}] \quad \text{as} \quad D \to \infty. \quad (46b)$$

Since $\theta_b = \sin \pi z \cos \alpha x f_b(y)$, equation (46b) shows an exponential decay of temperature disturbance in the semi-infinite conducting medium along the negative $y$-axis. It follows that the convection-induced thermal perturbations can only penetrate a short distance through the block. For example, if we define the penetration depth $Y_p$ to be the distance over which a thermal disturbance travels before it decays to 5% of its original value, then $Y_p \simeq 0.55$ when $K = 1$ and $\alpha = \alpha_c$. Beyond this distance the temperature field is represented basically by a linear temperature increase with depth due to conduction processes in the block. As a result, positioning the linear temperature distribution at any $y \leqslant -Y_p$ has little effect on the flow characteristics in the porous slab. This explains the extremely weak dependence of critical parameters on $D$ for $D \geqslant Y_p$, as exhibited in Figs. 3(a) and (b).

Figures 5(a)–(c) display isotherms at the onset of convection in the porous slab and one of its neighboring blocks at the vertical level $z = -1/2$, for the special case of $D \to \infty$, $\varepsilon = 0.1$, when $K = 0.5$, 1.0 and 2.0. In each of the three figures, the slab length $H_1$ is chosen to be equal to one critical wavelength for the particular $K$-value so that the convection pattern corresponds to global critical conditions. The number on each isotherm indicates the disturbance temperature given by equations (9) and (15). A normalized value of minus one has been assigned to the isotherm tangent to the interface between the slab and block at the mid-point of the slab. Other isotherm values measure the disturbance relative to this normalized isotherm. In the middle portion of the slab, the fluid descends in a three-dimensional convection cell with negative disturbance temperature. At the same time the warmer fluid at the bottom flows upwards near the endwalls, causing a positive temperature disturbance. This basic convection pattern will repeat if the slab length is increased by integer multiples. If the slab length differs slightly from an integer number of critical wavelengths, the number of cells $m$ in the slab remains the same as long as $H_{1tr}(m) \leqslant H_1 \leqslant H_{1tr}(m+1)$. However, the isotherm pattern in each cell will be slightly stretched or contracted in the $x$-direction. On the other hand, large changes in the slab length will cause the number of cells to be changed each time a transition point in the wave fitting condition (44) is exceeded.

The non-dimensional temperatures on isotherms are given by equations (6) and (14). It should be noted that the actual amplitude of the disturbances cannot be obtained from linear theory. Rather, one can ascertain only relative variations between one part of the field and another.

The influence of the thermal conductivity ratio $K$ on the horizontal temperature field in the slab–block system can be understood by examining Figs. 5(a)–(c). Comparing the three figures, one concludes that decreasing $K$, and hence reducing the sidewall heat transfer, results in wider convection cells. In addition one may note that the temperature gradient across the slab is less pronounced for small values of $K$, implying that the flow pattern is less strongly three-dimensional. This result agrees with that reported in ref. [6]

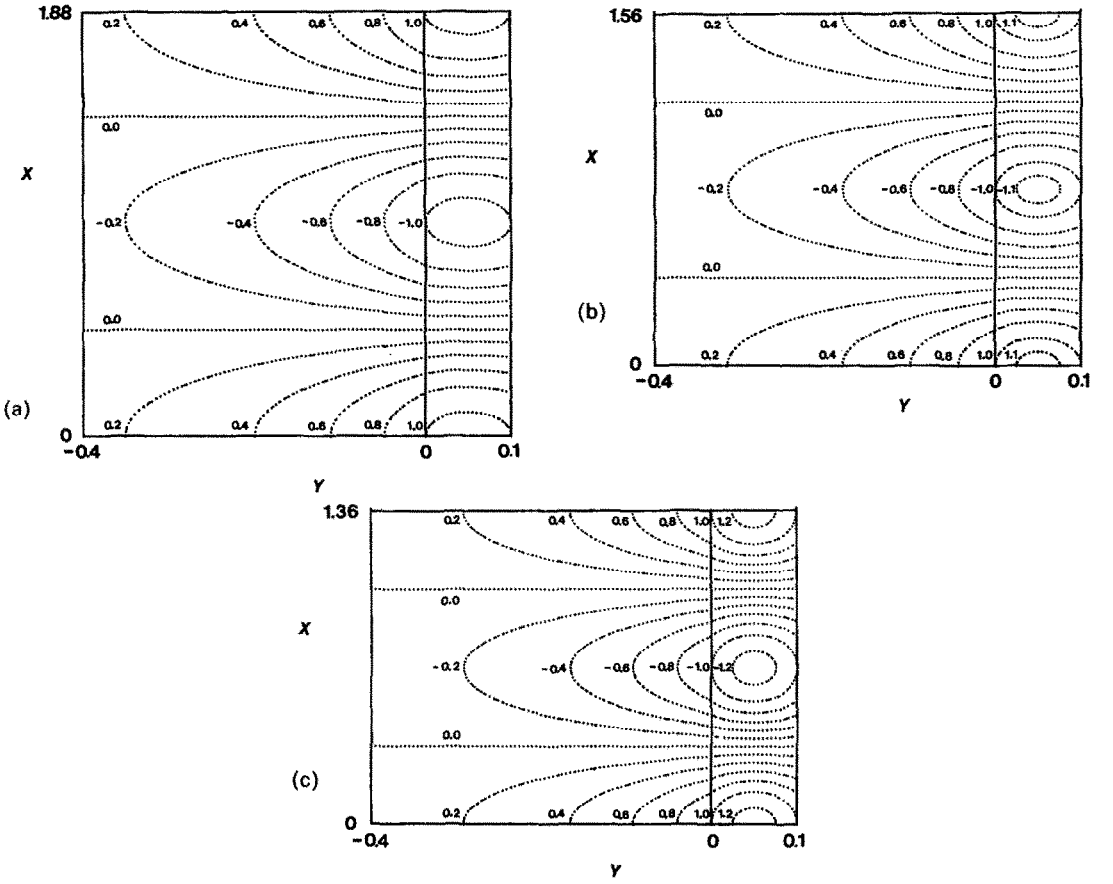


FIG. 5. Isotherm patterns (constant $\theta$-values) in the horizontal plane $z = -0.5$ for $D \to \infty$ and $\varepsilon = 0.1$. Numerical values are relative to a normalized value of unity on the slab–block interface: Case (a) $K = 0.5$; Case (b) $K = 1.0$; Case (c) $K = 2.0$.

and is reasonable since in the limiting case of insulated sidewalls, $K = 0$, one obtains purely two-dimensional convection cells.

It may be noted in Fig. 5 that the penetration distance of a given thermal disturbance in the block is largest when $K$ is a minimum, which corresponds to a minimum wave number $\alpha$. This result arises from equation (46b), which implies that the non-dimensional temperature decay length is proportional to $1/(\pi^2+\alpha^2)^{1/2}$. The implicit dependence of the penetration depth on $K$ through wave number $\alpha$ becomes weaker as the slab aspect ratio $\varepsilon$ is decreased, due to the $O(\varepsilon)$ dependence of the $\alpha_c$ on $K$ (c.f. equation (43)).

The continuous isotherm lines at the slab sidewall represent continuity in temperature distribution across the slab–block interface. The slopes of these isotherms, on the other hand, are not usually continuous at the interface. In fact, the slope of an isotherm is given by

$$\left(\frac{dx}{dy}\right)_{\theta=\text{const}} = -\frac{\theta_y}{\theta_x}. \tag{47}$$

At the slab–block interface $\theta_x = \theta_{bx}$, and $\theta_y = K\theta_{by}$. Thus

$$\left[\left(\frac{dx}{dy}\right)_{\theta=\text{const}}\right]_{y=0^+} = K\left[\left(\frac{dx}{dy}\right)_{\theta_b=\text{const}}\right]_{y=0^-}. \tag{48}$$

We conclude from equation (48), that unless $K = 1$, there is a jump in slope of the isotherms across the slab–block interface, as exhibited in Figs. 5(a) and (c); the exceptional case of continuous gradient of the isotherm contours at the slab–block interface is given in Fig. 5(b).

Finally, we consider the system in Fig. 1 when the block width is comparable to that of the slab. The solutions described above are not uniformly valid when $D = O(\varepsilon)$. Asymptotic results for this case, using $\bar{D} = D/\varepsilon$ indicate that the scalings $\bar{R} = \varepsilon^2 R$ and $\bar{\alpha} = \varepsilon^{1/2}\alpha$ identical to those found in refs. [5, 6] are required. Then

$$\bar{R} = \bar{R}_0 + \varepsilon\bar{R}_1 + O(\varepsilon^2) \tag{49}$$

where

$$\bar{R}_0^{1/2} \tan(\bar{R}_0^{1/2}/2) = K/\bar{D} \tag{50}$$

$$\bar{R}_1 = \frac{8\pi^2}{\bar{\alpha}^2}\frac{(K/\bar{D})^2}{\bar{R}_0 + 2(K/\bar{D}) + (K/\bar{D})^2}$$

$$+\bar{\alpha}^2\left\{1+\frac{4\bar{R}_0(K/\bar{D})\bar{D}^2}{3[\bar{R}_0+2(K/\bar{D})+(K/\bar{D})^2]}\right\}. \quad (51)$$

The above results are similar to equations (16), (18) and (19) in ref. [6], where the scaled Biot number $\bar{B}$ plays the role of $K/\bar{D}$. The underlying reason for this similarity is that for $D = O(\varepsilon)$, block conduction in the $y$-direction dominates that in the $x$-direction. The remaining effect of the small $x$-conduction in the thin block is accounted for by the second term in the curly bracket in equation (51), which does not appear in the results of ref. [6]. As $\bar{D} \to 0$ the results in ref. [5] are obtained. This demonstrates that when the block thickness is like that of the slab, fully three-dimensional high wave number solutions in the conducting block can be sustained.

## 4. CONCLUSION

This paper describes a study of the onset of natural convection in a finite, thin, vertically oriented saturated porous slab sandwiched between two impermeable conducting blocks. Several relevant parameters involved in the analyses are: $\varepsilon$ = slab width/height, $D$ = block width/height, and $K$ = block thermal conductivity/saturated porous matrix thermal conductivity. Our study shows that the presence of two contiguous conducting blocks changes the stability properties in the porous slab dramatically, due to the thermal interactions in the composite system. When $K = O(1)$, $D \gg O(\varepsilon)$, the critical Rayleigh number $R_c \sim O(1/\varepsilon)$. The corresponding convection mode consists of weakly three-dimensional square cells with critical wavelength $l_c \sim O(1)$. The sidewall heat exchange with the conducting blocks, which can be enhanced by either increasing $K$ or decreasing $D$, continues to be a strongly stabilizing effect. When $D = O(\varepsilon)$, tall, thin, three-dimensional finger-like cells, $l_c \sim O(\varepsilon^{1/2})$, are formed at a much higher Rayleigh number, $R_c \sim O(1/\varepsilon^2)$.

*Acknowledgement*—This work was supported by a grant from the National Science Foundation MEA-8011730. Additional support was provided by the Council on Research and Creative Work of the University of Colorado, Boulder.

## REFERENCES

1. J. L. Beck, Convection in a box of porous material saturated with fluid, *Physics Fluids* **15,** 1377–1383 (1972).
2. A. Zebib and D. R. Kassoy, Onset of natural convection in a box of water-saturated porous media with large temperature variation, *Physics Fluids* **20,** 4–9 (1977).
3. R. P. Lowell and C.-T. Shyu, On the onset of convection in a water-saturated porous box: effect of conducting walls, *Lett. Heat Mass Transfer* **5,** 371–378 (1978).
4. H. D. Murphy, Convective instabilities in vertical fractures and faults, *J. geophys. Res.* **84,** 6121–6130 (1979).
5. D. R. Kassoy and B. Cotte, The effects of sidewall heat loss on convection in a saturated porous vertical slab, *J. Fluid Mech.* **152,** 361–378 (1985).
6. P. D. Weidman and D. R. Kassoy, The influence of sidewall heat transfer on convection in a confined saturated porous medium, *Physics Fluids* **29,** 349–355 (1986).
7. D. R. Kassoy and A. Zebib, Convection fluid dynamics in a model of a fault zone in the Earth's crust, *J. Fluid Mech.* **88,** 769–797 (1978).
8. K. P. Goyal and D. R. Kassoy, A plausible two-dimensional vertical model of the East Mesa geothermal field, California, *J. geophys. Res.* **86,** 10719–10733 (1981).
9. J. P. Holman, *Heat Transfer*, p. 538. McGraw-Hill, New York (1981).

## APPENDIX

First-order terms for expanded critical Rayleigh number and critical wave number are listed below

$$\hat{R}^*_{1c} = \frac{2K\alpha_{1c}}{\alpha_{0c}^3}[\Lambda(\Lambda^2-3\pi^2)\coth(D\Lambda) - D\alpha_{0c}^2\,\mathrm{csch}^2(D\Lambda)] + \frac{3-K^2\coth^2(D\Lambda)}{3}\frac{\Lambda^4}{\alpha_{0c}^2} \quad (A1)$$

$$\alpha_{1c} = -\frac{1}{2K}\left\{\frac{2\Lambda^2(\Lambda^2-2\pi^2)[3-K^2\coth^2(D\Lambda)]}{3(\Lambda^2-\pi^2)^{3/2}} + \frac{2K^2D\Lambda^3\cosh(D\Lambda)}{3(\Lambda-\pi^2)^{1/2}\sinh^3(D\Lambda)}\right\} \Bigg/ \left\{\left[\frac{3\pi^2(\pi^2+\Lambda^2)}{\Lambda(\Lambda^2-\pi^2)^2} + 4D^2\Lambda\frac{\coth(2D\Lambda)}{\sinh(2D\Lambda)}\right]\coth(D\Lambda) + \left[\frac{D(5\pi^2-2\Lambda^2)}{\Lambda^2-\pi^2} + \frac{2D^2\Lambda}{\sinh(2D\Lambda)}\right]\mathrm{csch}^2(D\Lambda)\right\} \quad (A2)$$

where

$$\Lambda = (\pi^2+\alpha_{0c}^2)^{1/2}. \quad (A3)$$

## CONVECTION DANS UNE COUCHE VERTICALE DE MATERIAU POREUX SATURE ENTRE DEUX BLOCS CONDUCTEURS IMPERMEABLES

**Résumé**—On considère la convection naturelle dans une couche verticale de matériau poreux. Cette couche est serrée entre deux blocs conducteurs imperméables de dimension finie. Une différence de température est imposée verticalement entre les surfaces horizontales supérieure et inférieure de la couche et des blocs et une distribution linéaire de température est imposée sur les faces verticales externes des blocs. Cette configuration modélise la convection dans une zone rocheuse fracturée et saturée. Une analyse de stabilité linéaire est développée à la fois pour la convection dans la couche et la conduction dans les blocs. L'objectif de l'étude est d'obtenir le nombre de Rayleigh critique et le mode de convection dans la couche. Lorsque les épaisseurs du bloc et de la couche sont petites en comparaison des deux autres dimensions, on trouve un grand nombre de petites cellules serrées tridimensionnelles. Au contraire, un bloc de relativement grande épaisseur favorise la formation de cellules à grande longueur d'onde, faiblement tridimensionnelle dans la couche à un nombre de Rayleigh plus faible. La différence est reliée au caractère de la distribution de température dans le bloc solide.

## DAS EINSETZEN DER KONVEKTION IN EINEM SENKRECHTEN SPALT AUS EINEM GESÄTTIGTEN PORÖSEN MEDIUM ZWISCHEN ZWEI UNDURCHLÄSSIGEN, WÄRMELEITENDEN KÖRPERN

**Zusammenfassung**—Das Einsetzen der Konvektion in einem senkrechten, endlich dünnen Spalt, der mit gesättigtem, porösen Material gefüllt ist, wird betrachtet. Der Spalt ist zwischen zwei endlichen, undurchlässigen, wärmeleitenden Körpern eingebettet. Eine Temperaturdifferenz wird zwischen der horizontalen oberen und unteren Begrenzungsfläche der Anordnung aufgeprägt, ebenso eine linear verlaufende Temperaturverteilung auf den senkrechten Seitenflächen. Mit dieser Anordnung wird die Konvektion in Geröllschichten modelliert, wie sie in Verwerfungen auftreten. Eine lineare Stabilitätsanalyse wird sowohl für die Konvektion im Spalt als auch für die Wärmeleitung in den Körpern entwickelt. Ziel der Untersuchung ist, die kritische Rayleigh-Zahl und die Art der Konvektion im Spalt zu bestimmen. Wenn Spalt- und Festkörperdicke klein sind im Verhältnis zu den anderen beiden Abmessungen, beobachtet man eine große Zahl dünner, langer, dreidimensionaler Zellen. Dagegen führt ein breiter Festkörper zu nur gering ausgeprägten dreidimensionalen Zellen größerer Wellenlänge bei viel kleineren Rayleigh-Zahlen. Der Unterschied hängt von der Art der Temperaturverteilung im Festkörper ab.

## ВОЗНИКНОВЕНИЕ КОНВЕКЦИИ В ВЕРТИКАЛЬНОЙ ПЛАСТИНЕ НАСЫЩЕННОГО ПОРИСТОГО МАТЕРИАЛА МЕЖДУ ДВУМЯ НЕПРОНИЦАЕМЫМИ ТЕПЛОПРОВОДЯЩИМИ БЛОКАМИ

**Аннотация**—Рассматривается возникновение естественной конвекции в тонкой вертикальной пористой пластине, помещенной между двумя непроницаемыми проводящими блоками конечного размера. Существует перепад температуры по вертикали между верхней и нижней горизонтальными поверхностями пластины и блоков, а на наружных вертикальных поверхностях блоков задается линейное распределение температуры. Такая конфигурация используется для моделирования конвекции в насыщенной, заполненной раздробленной породой зоне, подобной зоне сбросообразования. Линейный анализ устойчивости проведен для конвекции в пластине и теплопроводности в блоке. Цель исследования—определить критическое число Рэлея и режим конвекции в пластине. В случае, когда поперечные размеры блока и пластины малы по сравнению с двумя другими размерами, обнаружено большое число высоких узких трехмерных ячеек. В отличие от вышеуказанного случая блок с относительно большой шириной способствует образованию в пластине слабовыраженных трехмерных ячеек с большой длиной волны при значительно более низких значениях числа Рэлея. Это различие связано с распределением температуры в твердом блоке.